FREQUENCY-DEPENDENCE OF RELATIVE PERMEABILITY IN STEEL

N. Bowler

Iowa State University, Center for Nondestructive Evaluation,
Applied Sciences Complex II, 1915 Scholl Road, Ames, IA 50011, USA

ABSTRACT. A study to characterize metal plates by means of a model-based, broadband, four-point potential drop measurement technique has shown that the relative permeability of alloy 1018 low-carbon steel is complex and a function of frequency. A magnetic relaxation is observed at approximately 5 kHz. The relaxation can be described in terms of a parametric (Cole-Cole) model. Factors which influence the frequency, amplitude and breadth of the relaxation, such as applied current amplitude, sample geometry and disorder (e.g. percent carbon content and surface condition), are considered.

INTRODUCTION

A study to characterize metal plates by means of a model-based, broadband, four-point potential drop measurement technique [1] has shown that the relative permeability, μ, of an alloy 1018 carbon-steel plate is complex and a function of frequency:

$$\mu(\omega) = \mu'(\omega) + i\mu''(\omega), \tag{1}$$

with $\omega = 2\pi f$ being angular frequency. For measurements made in the frequency range 1 Hz to 100 kHz, a clear relaxation in the relative permeability is observed at around 5 kHz, with the real part declining from a value of approximately $\mu' = 280$ at low frequencies (1 to 10 Hz), depending on the amplitude of the injected current, to approximately 90 at 100 kHz. Possible mechanisms responsible for this effect include phase lag in the motion of magnetic domain walls, with respect to the applied alternating current injected into the plate [2], or the presence of a surface region in which the material structure and its electromagnetic properties have been modified, compared with the bulk, for example by processing methods such as cold-rolling. The need for a complex, frequency-dependent magnetic permeability has also been recognized in studies on various ferromagnetic metal plates subjected to a homogenous time-harmonic magnetic field, with impedance measurements made by a pick-up coil wrapped around the specimen [3].

Here, the observed magnetic relaxation is characterized in terms of a parametric model [2]. Factors which influence the frequency, amplitude and breadth of the relaxation, such as sample geometry, amplitude of the applied current and disorder in the steel (e.g. percent carbon content and surface condition), are considered.
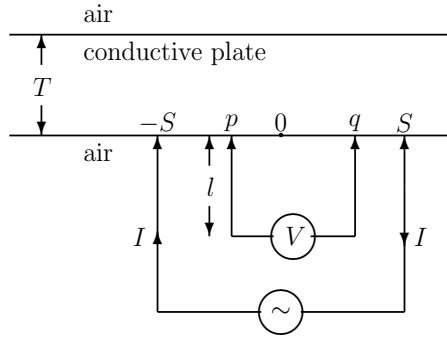
FIGURE 1: Four point probe in contact with a conductive plate. The probe points are arranged along a straight line. I is the amplitude of the applied alternating current.

A proper understanding of the observed frequency-dependence of μ is important for correct interpretation of alternating-current potential drop (ACPD) measurements for the purpose of characterizing surface treatments such as case-hardened layers in steels.

SPECIMEN

The chemical composition of the alloy 1018 low-carbon steel plate is given in Table 1. The thickness of the plate was measured using digital calipers: $T = 6.30 \pm 0.01$ mm. Other dimensions are 616×619 mm. It was not possible to anneal the specimen due to its large size. It was attempted to demagnetize the plate point-by-point using a C-core magnet on its surface, since it was too large to fit inside readily-available demagnetizing coils. This method may leave residual magnetization in local regions of the plate.

FOUR-POINT ALTERNATING CURRENT POTENTIAL DROP EXPERIMENT

A schematic diagram of a four-point probe in contact with a conductive plate is shown in Figure 1. Elsewhere it has been derived that, for this configuration, the voltage V measured between pick-up points at p and q can be expressed [1]

$$V = \frac{I}{2\pi} \left[-\frac{ik}{\sigma} \coth(ikT) + i\omega\mu_0 l \right] \ln \left[\frac{(S-p)(S+q)}{(S+p)(S-q)} \right], \qquad T < 0.3S. \qquad (2)$$

In equation (2), $k = (1+i)/\delta$ where $\delta = (2/\omega\mu_0\mu\sigma)^{1/2}$ is the electromagnetic skin depth in the conductor, $\mu_0 = 4\pi \times 10^{-7}$ H/m is the permeability of free space, μ and σ are the relative magnetic permeability and conductivity of the plate, respectively, and I is the amplitude of the alternating current. Probe dimensions are shown in Figure 1.

A series expansion analysis of equation (2) [1] permits derivation of the following expression, which describes a quasi-static regime in which the measured voltage is approximately real and constant, bounded by frequency f_s whose value is chosen depending on the level of

TABLE 1: Chemical composition (weight %) of alloy 1018 low-carbon steel.

carbon	0.15 - 0.20
manganese	0.6 - 0.9
sulfur	0.05 maximum
phosphorus	0.04 maximum
iron	remainder

TABLE 2: Probe parameters.

S (mm)	25.454 ± 0.005
p (mm)	-10.152 ± 0.005
q (mm)	10.162 ± 0.005
l (mm) (fitted value)	0.15 ± 0.1
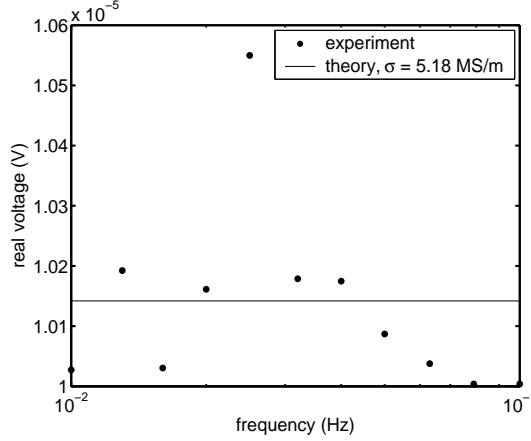
FIGURE 2: ACPD voltage measurements compared with theory in the quasi-static regime ($f <$ 0.46 Hz).

accuracy required.

$$V_{\mathrm{s}} = \frac{I}{2\pi\sigma T} \ln\left[\frac{(S-p)(S+q)}{(S+p)(S-q)}\right], \qquad f < f_{\mathrm{s}}. \tag{3}$$

For 0.1% accuracy in V_{s},

$$f_{\mathrm{s}} = \frac{3}{20\sqrt{2}\pi\mu\sigma T^2}. \tag{4}$$

From experimental results described later it will be seen that $f_{\mathrm{s}} \approx 0.46$ Hz for this plate.

Four sprung, point contacts were mounted in a plastic support block. The four points were arranged along a straight line, and the separation of the contacts was measured using a traveling microscope. With reference to Figure 1, the dimensions of the probe are listed in Table 2. Other details of the experimental arrangement have been described elsewhere [1].

DETERMINATION OF PLATE CONDUCTIVITY

The conductivity of the plate was determined from comparison of ACPD voltage measurements in the quasi-static regime with theoretical expressions (3) and (4), Figure 2. Details of the procedure and analysis of uncertainties are given in reference [4]. The conductivity of the plate was determined to be 5.18 ± 0.04 MS/m.

DETERMINATION OF PLATE PERMEABILITY

With known conductivity, the permeability of the plate can be obtained by adjusting $\mu(\omega)$ in equation (2) to achieve agreement between experimentally-measured and calculated voltage values. This was done on a point-by-point basis in the frequency range 1 Hz to 100 kHz to obtain the curves shown in Figure 3. A strong relaxation in $\mu(\omega)$ is seen at approximately 5 kHz. The low-frequency limiting value of $\mu(\omega)$ depends somewhat on the amplitude of the drive current. The drive current itself is real and constant over the majority of the measurement frequency range, but reduces in magnitude and undergoes a phase shift at higher frequencies, as shown in Figure 4.
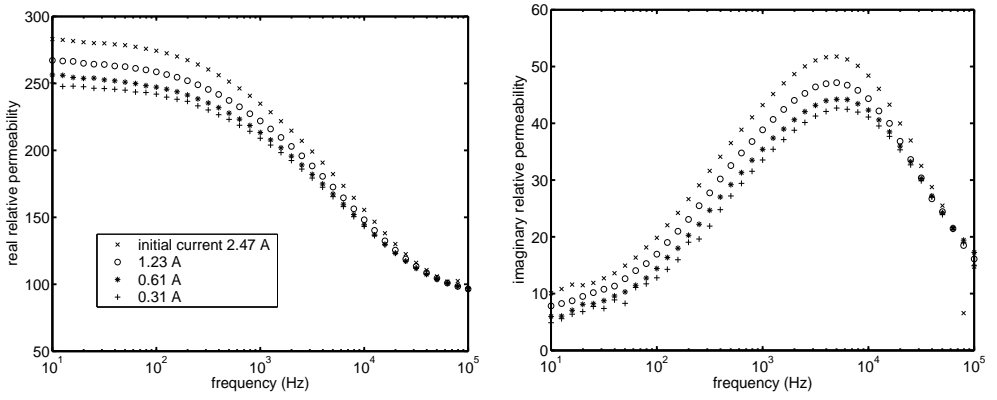
FIGURE 3: Real and imaginary parts of complex permeability as a function of frequency.
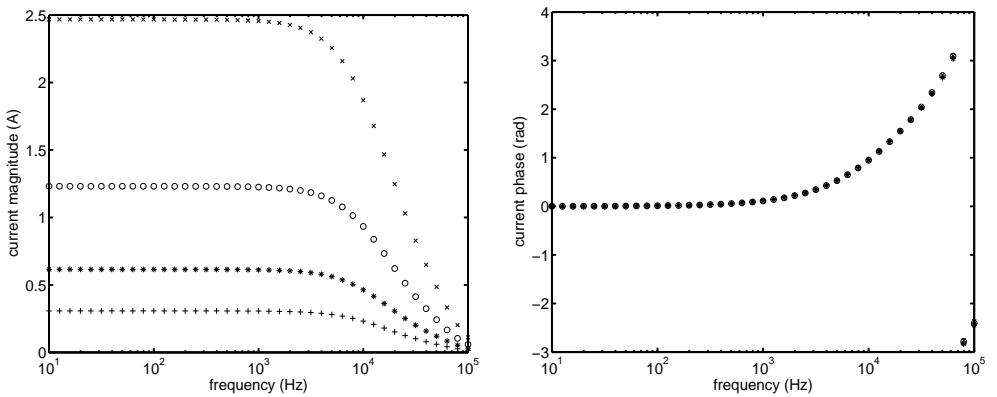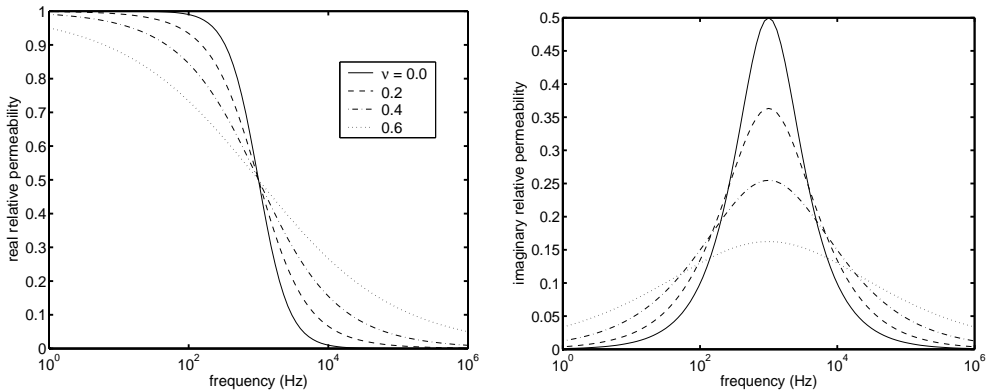

FIGURE 4: Magnitude and phase of driving current as a function of frequency.

FIGURE 5: Real and imaginary parts of relative permeability as a function of frequency, calculated using equation (5), for various values of the parameter ν. The relaxation time t is chosen arbitrarily to be 1 kHz. Similarly, $\mu'(0) = 1$ and $\mu'_\infty = 0$.

TABLE 3: Low-frequency, real permeability, $\mu'(0)$.

initial current (A)	$\mu'(0)$
2.47	285 ± 2
1.23	269 ± 2
0.61	259 ± 2
0.31	251 ± 2

PERMEABILITY MODEL

For a constant amplitude of applied magnetic field, the complex permeability may be written [2]

$$\mu(\omega) = \frac{\mu'(0) - \mu'_\infty}{1 - i\omega\tau(\omega)} + \mu'_\infty, \tag{5}$$

in which $\mu'(0)$ and μ'_∞ are the low- and high-frequency, constant, real relative permeability values for the relaxation process, respectively, and $\tau(\omega)$ represents a relaxation 'time' that may be complex. Equation (5) reduces to the Debye form of relaxation if $\tau(\omega) = t = $ constant. The Cole-Cole representation is obtained for

$$\tau(\omega) = \omega^{-\nu} t^{1-\nu} e^{i\nu\pi/2}, \qquad \nu \geq 0. \tag{6}$$

The Debye form is recovered from (6) when $\nu = 0$. In Figure 5, μ is plotted for various values of the parameter ν. It can be seen that increasing ν gives broader relaxation while reducing the magnitude of the loss peak in the imaginary permeability. In Figure 6, parametric curves are compared with experimental data. Calculated curves shown in Figure 6 are obtained with parameters $\mu'_\infty = 78$, $1/t = 5$ kHz and $\nu = 0.4$. The same data are displayed in a permeability-plane plot in Figure 7. For each value of initial applied current, $\mu'(0)$ is obtained by taking the mean of the first few low-frequency data points. The values obtained are listed in Table 3 and plotted as a function of initial applied current in Figure 8.

DISCUSSION

The experimental data for μ' is reproduced very well by the theoretical curves except in the highest frequency decade (10^4 to 10^5 Hz). The magnitude of the peaks in μ'' is also well-reproduced by theory, whereas the experimental data exhibits some asymmetry. These
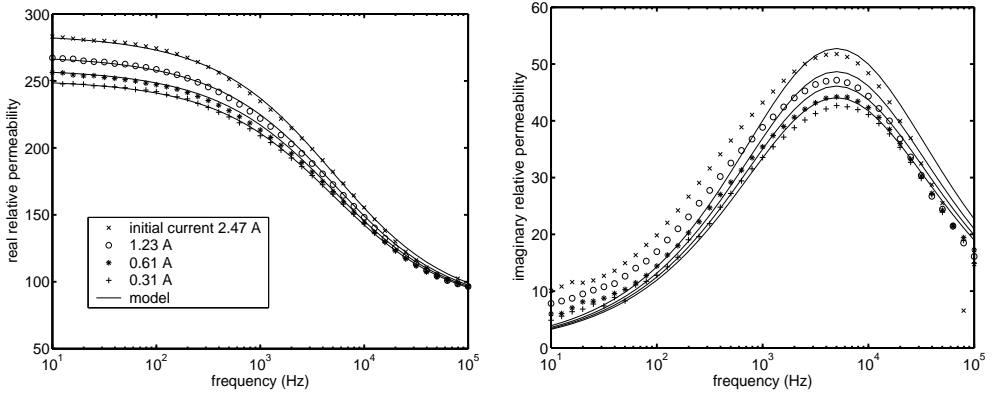
FIGURE 6: Experimental and modelled real and imaginary parts of relative permeability as a function of frequency. Modelled values are calculated using equations (5) and (6), with parameters $\mu'_\infty = 78$, $1/t = 5$ kHz and $\nu = 0.4$. $\mu'(0)$ for each value of initial applied current is listed in Table 3.
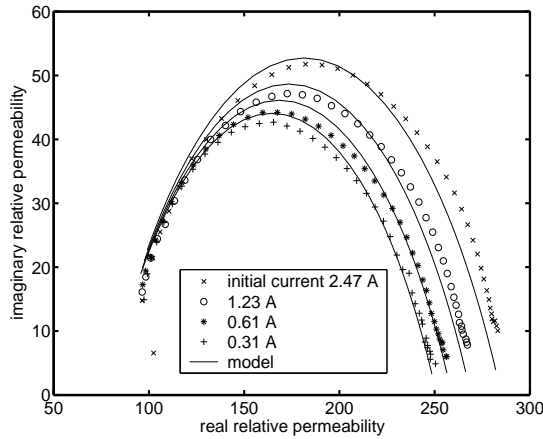
FIGURE 7: Permeability-plane plot of experimental and modelled complex permeability.
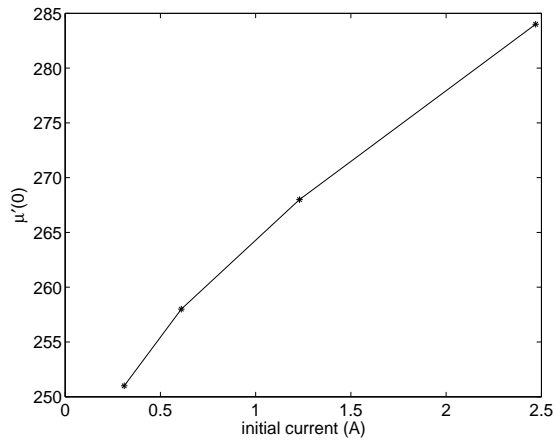
FIGURE 8: Low-frequency, real permeability, $\mu'(0)$, as a function of initial applied current amplitude.
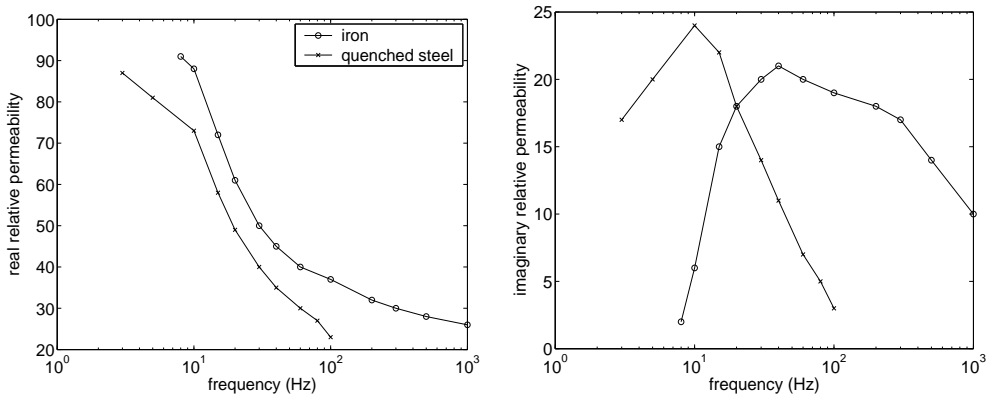
FIGURE 9: Real and imaginary parts of complex permeability as a function of frequency for measurements on iron and quenched steel. Data is taken from reference [3].

discrepancies may be attributed to the significantly reduced amplitude of the drive-current in the frequency range 10^4 to 10^5 Hz, as shown in Figure 4, since the model assumes constant amplitude of the applied magnetic field, H, whereas H is proportional to I. In addition, injecting current by means of a four-point probe clearly gives rise to a spatially-varying magnetic field whose amplitude at any one field point depends on the geometry of the specimen and the probe. It is also possible that microstructural changes near the surface of the specimen, for example due to cold-finishing, may give rise to changes in the electromagnetic properties of the steel in a surface region. This means that μ may also vary as a function of depth in the specimen, in a way not represented by equations (5) and (6).

It is not surprising that the observed relaxation is broader (with $\nu = 0.4$) than a Debye relaxation ($\nu = 1$) since most physical systems exhibit microstructural inhomogeneities which give rise to a distribution of relaxation times, here embedded in the function $\tau(\omega)$.

The variation of $\mu'(0)$ as a function of the amplitude of the initial current, Table 3 and Figure 8, is explained by the fact that the magnetic field, H, in the specimen is proportional to the applied current. As the applied current changes, H also changes and a different point on the magnetization curve for the material (the curve of B versus H) is reached. The value of $\mu'(0)$ changes according to the slope of the magnetization curve.

CONCLUSION

Magnetic relaxation has been observed in measurements made on an alloy 1018 carbon-steel plate by a model-based four-point alternating-current potential drop technique. A possible mechanism responsible for this phenomenon is phase lag of domain wall motion, either bowing or movement between pinning sites, with respect to the applied field. The phenomenon may therefore be expected to be disorder-dependent, related to the density of pinning sites in the material, which in turn may be related to the percent carbon content in steel, for example. Indeed, relaxation in μ has not been observed in similar experiments on spring steel [1] and an independent study has shown a difference in behavior between iron and quenched steel [3], as shown in Figures 9 and 10. Surface condition and processing history of the sample may also play a role, since both of these influence the density and nature of domain-wall pinning sites. The phenomenon at work here may be responsible for the inability to fit eddy-current impedance data, taken on iron and high-purity nickel samples, using standard models assuming homogeneous material properties [5]. Further work is necessary to identify precisely the mechanism(s) responsible for the observed frequency-dependence of μ.
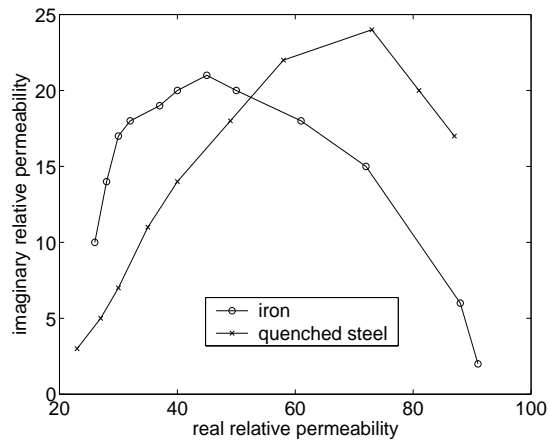
FIGURE 10: Permeability-plane plot of data shown in Figure 9.

ACKNOWLEDGMENTS

REFERENCES

1. N. Bowler and Y. Huang, *IEEE Trans. Mag.* **41**, 2102–2110 (2005).
2. J. Sláma, P. Krivošík and V. Jančárik, *J. Magnetism and Magnetic Materials* **215–216**, 641–643 (2000).
3. V. A. Sandovskii, V. V. Dyakin and M. S. Dudarev, *Russian J. Nondestr. Testing* **33**, 52–55 (1997).
4. N. Bowler and Y. Huang, *Meas. Sci. Tech.*, accepted August 2005.
5. J. C. Moulder, C.-C. Tai, B. F. Larson and J. H. Rose, *IEEE Trans. Mag.* **34**, 505–514 (1998).